Catalytic Generation of Oxalate through a Coupling Reaction of Two CO_2 Molecules Activated on $[(Ir(\eta^5\text{-}C_5Me_5))_2(Ir(\eta^4\text{-}C_5Me_5)CH_2CN)(\mu_3\text{-}S)_2]$

Koji Tanaka,*,† Yoshinori Kushi,† Kiyoshi Tsuge,† Kiyotsuna Toyohara,† Takanori Nishioka,‡ and Kiyoshi Isobe‡

Institute for Molecular Science, Myodaiji, Okazaki 444, Japan, and Department of Material Science, Faculty of Science, Osaka City University, Sugimotochou, Sumiyoshi-ku, Osaka 558, Japan

Received February 26, 1997[⊗]

Electrochemical reduction of $[(Ir(\eta^5\text{-}C_5Me_5))_3(\mu_3\text{-}S)_2](BPh_4)_2$ ($[Ir_3S_2](BPh_4)_2$) in CO_2-saturated CH_3CN at −1.30 V (*vs* Ag/AgCl) produced $C_2O_4^{2-}$ and $[(Ir(\eta^5\text{-}C_5Me_5))_2(Ir(\eta^4\text{-}C_5Me_5)CH_2CN)(\mu_3\text{-}S)_2]^+$ ($[Ir_3S_2CH_2CN]^+$). The crystal structure of $[Ir_3S_2CH_2CN](BPh_4)$ by X-ray analysis revealed that a linear CH_2CN group is linked at the exo-position of a C_5Me_5 ligand, and the $C_5Me_5CH_2CN$ ligand coordinates to an Ir atom with an η^4-mode. The cyclic voltammogram of $[Ir_3S_2CH_2CN]^+$ in CH_3CN under CO_2 exhibited a strong catalytic current due to the reduction of CO_2, while that of $[Ir_3S_2]^{2+}$ did not show an interaction with CO_2 in the same solvent. The reduced form of $[Ir_3S_2CH_2CN]^+$ works as the active species in the reduction of CO_2. The IR spectra of $[Ir_3S_2CH_2CN]^+$ in CD_3CN showed a reversible adduct formation with CO_2 and also evidenced the oxalate generation through the reduced form of the CO_2 adduct under the controlled potential electrolysis of the solution at −1.55 V. A coupling reaction of two CO_2 molecules bonded on adjacent μ_3-S and Ir in $[Ir_3S_2CH_2CN]^0$ is proposed for the first catalytic generation of $C_2O_4^{2-}$ without accompanying CO evolution.

Introduction

Activation of CO_2 on metal complexes is a continuing important subject from the viewpoint of utilization of CO_2 as a C1 resource. A variety of metal complexes have proven to be active for the generation of CO and/or HCOOH in the electro-[1] and photochemical reduction of CO_2.[2] There have been arguments concerning the precursors to HCOOH, because metal−OC(O)H,[3] −C(O)OH,[4] and −C(O)H[5] complexes have been proposed as the reaction intermediates. On the other hand, metal−CO complexes are generally accepted as precursors to CO generation.[1n,p,z,6] Transformation from metal−η^1-CO_2 complexes to metal−CO ones in the presence of proton donors takes place through metal−C(O)OH species (eq 1). It is worthy

$$[MCO_2]^{n+} \overset{H^+}{\rightleftharpoons} [MC(O)OH]^{(n+1)+} \overset{H^+}{\rightleftharpoons} [MCO]^{(n+2)+} \quad (1)$$

$$[MCO_2]^{n+} + CO_2 \rightarrow [MCO]^{n+2} + CO_3^{2-} \quad (2)$$

to note that the acidity of a proton donor (AH) in the equilibrium of eq 1 is largely enhanced by CO_2 due to the exothermal adduct formation between the conjugate base (A^-) and CO_2.[7a] With regard to structural changes of metal complexes in the equilibrium of eq 1, for a series of Ru−CO_2, Ru−C(O)OH, and Ru−CO complexes their molecular structures have been determined by X-ray analysis.[7] Besides metal−CO_2, −C(O)OH, and −CO complexes in the equilibrium of eq 1, the metal−$C(OH)_2$ species is also suggested in the transformation from metal−C(O)OH to metal−CO of eq 1.[8] In the absence of proton donors, an oxide transfer reaction from metal−CO_2 to CO_2 (eq 2) is responsible for the transformation of metal−CO_2 to metal−CO complexes in homogeneous reactions.

Recently, we have reported multielectron reduction of CO_2 accompanied with carbon−carbon bond formation by taking advantage of smooth CO_2/CO conversion on Ru in protic media (eq 1). Electrochemical reduction of $[Ru(bpy)(trpy)(CO)]^{2+}$

† Institute for Molecular Science.
‡ Osaka City University.
⊗ Abstract published in *Advance ACS Abstracts,* December 15, 1997.

(1) (a) Nakajima, H.; Mizukawa, T.; Nagao, H.; Tanaka, K. *Chem. Lett.* **1995**, 251. (b) Lam, K.-M.; Wong, K.-Y.; Yang, S.-M.; Che, C.-M. *J. Chem. Soc., Dalton Trans.* **1995**, 1103. (c) Costamagna, J.; Canales, J.; Vargas, J.; Ferraudi, G. *Pure Appl. Chem.* **1995**, *67*, 1045. (d) Herring, A. M.; Steffey, B. D.; Miedaner, A.; Wander, S. A.; DuBois, D. L. *Inorg. Chem.* **1995**, *34*, 1100. (e) Arana, C.; Keshavarz, M.; Potts, K. T.; Abruna, H. D. *Inorg. Chim. Acta* **1994**, *225*, 285. (f) Steffey, B. D.; Miedaner, A.; Maciejewski-Farmer, M. L.; Bernatis, P. R.; Herring, A. M.; Allured, V. S.; Carperos, V.; DuBois, D. L. *Organometallics* **1994**, *13*, 4844. (g) Szymaszek, A.; Pruchnik, F. *Rhodium Express* **1994**, *5*, 18. (h) Fujita, E.; Haff, J.; Sanzenbacher, R.; Elias, H. *Inorg. Chem.* **1994**, *33*, 4627. (i) Ogura, K.; Sugihara, H.; Yano, J.; Higasa, M. *J. Electrochem. Soc.* **1994**, *141*, 419. (j) Chardon-Noblat, S.; Collomb-Dunand-Sauthier, M.-N.; Deronzier, A.; Ziessel, R.; Zsoldos, D. *Inorg. Chem.* **1994**, *33*, 4410. (k) Christensen, P.; Hamnett, A.; Muir, A. V. G.; Timney, J. A.; Higgins, S. *J. Chem. Soc., Faraday Trans.* **1994**, *90*, 459. (l) Kimura, E.; Wada, S.; Shionoya, M.; Okazaki, Y. *Inorg. Chem.* **1994**, *33*, 770. (m) Kolodsick, K. J.; Schrier, P. W.; Walton, R. A. *Polyhedron* **1994**, *13*, 457. (n) Collomb-Dunand-Sauthier, M. N.; Deronzier, A.; Ziessel, R. *J. Chem. Soc., Chem. Commun.* **1994**, 189. (o) Haines, R. J.; Wittrig, R. E.; Kubiak, C. P. *Inorg. Chem.* **1994**, *33*, 4723. (p) Collomb-Dunand-Sauthier, M.-N.; Deronzier, A.; Ziessel, R. *Inorg. Chem.* **1994**, *33*, 2961. (q) Yoshida, T.; Tsutsumida, K.; Teratani, S.; Yasufuku, K.; Kaneko, M. *J. Chem. Soc., Chem. Commun.* **1993**, 631. (r) Tsai, J.-C.; Nicholas, K. M. *J. Am. Chem. Soc.* **1992**, *114*, 5117. (s) Arana, C.; Yan, S.; Keshavarz, M.; Potts, K. T.; Abruna, H. D. *Inorg. Chem.* **1992**, *31*, 3690. (t) Kimura, E.; Bu, X.; Shionoya, M.; Wada, S.; Maruyama, S. *Inorg. Chem.* **1992**, *31*, 4542. (u) Bruce, M. R. M.; Megehee, E.; Sullivan, B. P.; Thorp, H. H.; O'Toole, T. R.; Downard, A.; Pugh, J. R.; Meyer, T. J. *Inorg. Chem.* **1992**, *31*, 4864. (v) Christensen, P.; Hamnett, A.; Muir, A. V. G.; Timney, J. A. *J. Chem. Soc., Dalton Trans.* **1992**, 1455. (w) Ratliff, K. S.; Lentz, R. E.; Kubiak, C. P. *Organometallics* **1992**, *11*, 1986. (x) Graf, E.; Leitner, W. *J. Chem. Soc., Chem. Commun.* **1992**, 623. (y) Halmann, M. M., Ed.*Chemical Fixation of Carbon Dioxide*; CRC Press: London, 1993; p 67. (z) Sullivan, B. P., Krist, K., Guard, H. E., Eds. *Electrochemical and Electrocatalytic Reaction of Carbon Dioxide*; Elsevier Science Publishers BV: Amsterdam, 1993, and references cited therein.

S0020-1669(97)00232-2 CCC: $15.00
Published on Web 01/12/1998

(bpy = 2,2′-bipyridine) in EtOH/H_2O under CO_2 at −20 °C proceeds via Ru−CO_2, Ru−C(O)OH, Ru−CO, Ru−CHO, and Ru−CH_2OH species. The latter two function as precursors to not only H_2CO and CH_3OH but also HOOCCHO and $HOOCCH_2OH$ under the electrolysis conditions.[9] Similar electrochemical reduction of CO_2 catalyzed by $[Ru(bpy)_2(qu)(CO)]^{2+}$ (qu = quinoline) or $[Ru(bpy)(trpy)(CO)]^{2+}$ under aprotic conditions produced CO and CO_3^{2-} due to an oxide transfer reaction from the Ru−η^1-CO_2 intermediate to CO_2 (eq 2).[10] In these CO_2 reductions, neither HOOCCOOH nor $^-OOCCOO^-$ was formed irrespective of the presence and absence of proton donors. Thus, the CO_2/CO conversion through M−η^1-CO_2 and M−η^1-C(O)OH complexes (eqs 1 and 2) serves the reduction of CO_2 with a C−O bond cleavage, which, however, practically inhibits $C_2O_4^{2-}$ generation.

Oxalate production by one- or two-electron reduction of CO_2 is advantageous for carbon−carbon bond formation, since four and six electrons are consumed for the formation of HOOCCHO and $HOOCCH_2OH$ in the reduction of CO_2. Savéant et al. have found that anion radicals of aromatic nitriles and esters remarkably enhance the generation of oxalate in electrochemical reduction of CO_2.[11] The reaction is explained by an electrophilic attack of CO_2 to the oxygen or nitrogen of the anion radicals followed by dissociation of $CO_2^{\bullet-}$ by homolytic cleavage of the bonds and then the subsequent coupling of free $CO_2^{\bullet-}$. The redox potentials of aromatic nitriles and esters used as the catalysts in the CO_2 reduction are still quite negative and very close to that of $E°(CO_2/CO_2^-)$ at −2.21 V (*vs* SCE).[12] As similar to an electrophilic attack of CO_2 to anion radicals of aromatic nitriles and esters, basic ligands which possess a lone pair will undergo an attack of CO_2 to form adducts, in which the C−O bond will be much more stable than that of M−η^1-CO_2 adducts (eqs 1 and 2). Indeed, CO_2 activated on a μ_3-S ligand in $[Fe_6Mo_2(\mu_3\text{-}S)_8(SEt)_6(\mu_2\text{-}SEt)_3]^{5-}$ is utilized in electrochemical CO_2 fixation to RC(O)SR′ (R, R′ = alkyl, aryl), affording $RC(O)COO^-$ (eq 3).[13] Metal sulfur clusters with μ_3-S

$$RC(O)SR' + CO_2 + 2e^- \rightarrow RC(O)COO^- + R'S^- \quad (3)$$

moieties, therefore, may provide suitable reaction sites for the reduction of CO_2 without accompanying the C−O bond cleavage. We have briefly reported selective $C_2O_4^{2-}$ generation in electrochemical reduction of CO_2 in the presence of $[(Co(\eta^5\text{-}C_5H_5))_3(\mu_3\text{-}S)_2]^{2+}$,[14] $[(Rh(\eta^5\text{-}C_5Me_5))_3(\mu_3\text{-}S)_2]^{2+}$,[15] and $[(Ir(\eta^5\text{-}C_5Me_5))_3(\mu_3\text{-}S)_2]^{2+}$.[14] This paper describes details of the formation of $C_2O_4^{2-}$ in electrochemical reduction of CO_2 using $[(Ir(\eta^5\text{-}C_5Me_5))_3(\mu_3\text{-}S)_2](BPh_4)_2$ as a catalyst precursor.

Experimental Section

Materials. $[(Ir(\eta^5\text{-}C_5Me_5))_3(\mu_3\text{-}S)_2]^{2+}$ was prepared by the literature methods.[16] CH_3CN was distilled over calcium hydride. Gaseous $^{13}CO_2$ was generated by an addition of concentrated H_2SO_4 to $Ba^{13}CO_3$ (98 at. %), trapped at 77 K, and then allowed to evaporate slowly by warming to room temperature. Other chemicals were used as received.

Preparation of $[(Ir(\eta^5\text{-}C_5Me_5))_2(Ir(\eta^4\text{-}C_5Me_5)CH_2CN)(\mu_3\text{-}S)_2](BPh_4)$. A blue CH_3CN solution (5 cm^3) of $[(Ir(\eta^5\text{-}C_5Me_5))_3(\mu_3\text{-}S)_2]^0$ was prepared by two-electron reduction of $[(Ir(\eta^5\text{-}C_5Me_5))_3(\mu_3\text{-}S)_2](BPh_4)_2$ (101 μmol, 0.17 g) at −1.30 V (*vs* Ag|AgCl) in the presence of Me_4NBF_4 in CH_3CN under N_2 atmosphere. The color of the solution changed from blue to orange with the introduction of CO_2. The solution was further stirred for 2 h, and $(Me_4N)_2C_2O_4$ precipitated in a 40% yield (40 μmol, 9.5 mg). After the solvent was removed under a stream of CO_2, the residue was extracted with CH_2Cl_2 (3 × 10 cm^3). The solution was filtered, concentrated to ca. 10 cm^3 under CO_2, and then loaded onto an aluminum oxide column (Alumina Activated 300, Nacalai tesque). Elution with CH_3CN/CH_2Cl_2 (1:9 (v/v)) under N_2 gave orange and yellow bands. The yellow eluent contained $[(Ir(\eta^5\text{-}C_5Me_5))_3(\mu_3\text{-}S)_2](BPh_4)_2$. The orange eluent was concentrated to 5 cm^3. An addition of diethyl ether (10 cm^3) to the solution gave a reddish orange precipitate of $[(Ir(\eta^5\text{-}C_5Me_5))_2(Ir(\eta^4\text{-}C_5Me_5)CH_2CN)(\mu_3\text{-}S)_2](BPh_4)$ in a 44% yield (44 μmol). IR spectrum (KBr): $\nu(C{\equiv}N)$ 2238 cm^{-1}. ^1H NMR (270 MHz, CD_2Cl_2): δ 0.08 (s, 2H), 1.00 (s, 3H), 1.79 (s, 6H), 2.12 (s, 30H), 2.25 (s, 6H). FAB-mass spectrum (*m*/*z*): 1087 (M − BPh_4), 1047 (M − BPh_4 − CH_2CN).

Physical Measurements. Infrared spectra were obtained on a Shimadzu FTIR-8100 spectrophotometer. ^1H NMR was measured on a JEOL EX270 (270 MHz) spectrometer. Electronic spectra were measured on a Hewlett-Packard 8452A diode array spectrophotometer. FAB-mass and GC-mass spectra were obtained on a Shimadzu/Kratos Concept 1S and a Shimadzu GC-mass QP-1000EX, respectively. Electrochemical measurements were performed with a Hokuto Denko HAB-151 potentiostat and a Riken Denshi Co. F-72F *X*−*Y* recorder using a glassy-carbon disk working electrode (i.d. = 3 mm), a Pt auxiliary electrode, and an Ag|AgCl reference electrode purchased from BAS Co., Ltd.

X-ray Structure Analysis. The single crystals of $[(Ir(\eta^5\text{-}C_5Me_5))_2(Ir(\eta^4\text{-}C_5Me_5)CH_2CN)(\mu_3\text{-}S)_2](BPh_4)$ for the X-ray measurement were obtained by diffusing diethyl ether over a dichloromethane and acetone

(2) (a) Ogata, T.; Yamamoto, Y.; Wada, Y.; Murakoshi, K.; Kusaba, M.; Nakashima, N.; Ishida, A.; Takamuku, S.; Yanagida, S. *J. Phys. Chem.* **1995**, *99*, 11916. (b) Ishitani, O.; George, M. W.; Ibusuki, T.; Johnson, F. P. A.; Koike, K.; Nozaki, K.; Pac, C.; Turner, J. J.; Westwell, J. R. *Inorg. Chem.* **1994**, *33*, 4712. (c) Matsuoka, S.; Yamamoto, K.; Ogata, T.; Kusaba, M.; Nakashima, N.; Fujita, E.; Yanagida, S. *J. Am. Chem. Soc.* **1993**, *115*, 601. (d) Calzaferri, G.; Haedener, K.; Li, J. *J. Photochem. Photobiol., A* **1992**, *64*, 259. (e) Kimura, E.; Bu, X.; Shinomihya, M.; Wada, S.; Maruyama, S. *Inorg. Chem.* **1992**, *31*, 4542, and references cited therein.

(3) (a) Ratliff, K. S.; Lentz, R. E.; Kubiak, C. P. *Organometallics* **1992**, *11*, 1986. (b) Jeget, C.; Fouassier, M.; Mascett, J. *Inorg. Chem.* **1991**, *30*, 1521. (c) Jeget, C.; Fouassier, M.; Tranquille, M.; Mascett, J. *Inorg. Chem.* **1991**, *30*, 1529. (d) Pugh, J. R.; Bruce, M. R. M.; Sullivan, B. P.; Meyer, T. J. *Inorg. Chem.* **1991**, *30*, 86. (e) Sullivan, B. P.; Meyer, T. J. *J. Chem. Soc., Chem. Commun.* **1984**, 1244.

(4) (a) Ishida, H.; Fujiki, K.; Ohba, T.; Ohkubo, K.; Tanaka, T.; Terada, T.; Tanaka, T. *J. Chem. Soc., Dalton Trans.* **1990**, 2155. (b) Ishida, H.; Tanaka, K.; Morimoto, M.; Tanaka, T. *Organometallics* **1986**, *5*, 724. (c) Tanaka, K.; Morimoto, M.; Tanaka, T. *Chem. Lett.* **1983**, 901. (d) Choudhury, D.; Cole-Hamilton, D. J. *J. Chem. Soc., Dalton Trans.* **1982**, 1885. (e) Ishida, I.; Tanaka, K.; Tanaka, T. *Organometallics* **1987**, *6*, 181.

(5) Toyohara, K.; Nagao, H.; Mizukawa, T.; Tanaka, K. *Inorg. Chem.* **1995**, *34*, 5399.

(6) (a) Beley, M.; Collin, J.-P.; Ruppert, R.; Sauvage, J.-P. *J. Chem. Soc., Chem. Commun.* **1984**, 1315. (b) Beley, M.; Collin, J.-P.; Ruppert, R.; Sauvage, J.-P. *J. Am. Chem. Soc.* **1986**, *108*, 7461. (c) Lee, G. L.; Maher, J. M.; Cooper, N. J. *J. Am. Chem. Soc.* **1987**, *109* , 2956. (d) Lee, G. R.; Cooper, N. J. *Organometallics* **1985**, *4*, 794.

(7) (a) Tanaka, H.; Tzeng, B.-C.; Nagao, H.; Peng, S.-M.; Tanaka, K. *Inorg. Chem.* **1993**, *32*, 1508. (b) Toyohara, K.; Nagao, H.; Adachi, T.; Yoshida, T.; Tanaka, K. *Chem. Lett.* **1996**, 27.

(8) Bhugun, I.; Lexa, D.; Savéant, J.-M. *J. Am. Chem. Soc.* **1996**, *118*, 1769.

(9) (a) Nagao, H.; Mizukawa, T.; Tanaka, K. *Inorg. Chem.* **1994**, *33*, 3415. (b) Nagao, H.; Mizukawa, T.; Tanaka, K. *Chem. Lett.* **1993**, 955.

(10) Nakajima, H.; Kushi, Y.; Nagao, H.; Tanaka, K. *Organometallics* **1995**,*14*, 5093.

(11) Gennaro, A.; Isse, A. A.; Savéant, J.-M.; Severin, M.-G.; Vianello E. *J. Am. Chem. Soc.* **1996**, *118*, 7190.

(12) (a) Amatore, C.; Savéant, J.-M. *J. Am. Chem. Soc.* **1981**, *103*, 5021. (b) Gressin, J.-C.; Michelet, D.; Nadjo, L.; Saveant, J.-M. *Nouv. J. Chim.* **1979**, *3*, 545. (c) Desilvestro, J.; Pons, S. *J. Electroanal. Chem.* **1989**, *267*, 207.

(13) (a) Komeda, N.; Nagao, H.; Matsui, T.; Adachi, G.; Tanaka, K. *J. Am. Chem. Soc.* **1992**, *114*, 3625. (b) Nakamoto, M.; Tanaka, K.; Tanaka, T. *Bull. Chem. Soc. Jpn.* **1988**, *61*, 4099. (c) Tanaka, K.; Moriya, M.; Takaka, T. *Inorg. Chem.* **1986**, *25*, 835.

(14) Kushi, Y.; Nagao, H.; Nishioka, H.; Isobe, K.; Tanaka, K. *J. Chem. Soc., Chem. Commun.* **1995**, 1223.

(15) Kushi, Y.; Nagao, H.; Nishioka, H.; Isobe K.; Tanaka, K. *Chem. Lett.* **1994**, 2175.

(16) (a) Nishioka, T.; Isobe, K. *Chem. Lett.* **1994**, 1661. (b) Venturelli, A.; Rauchfuss, T. B. *J. Am. Chem. Soc.* **1994**, *116*, 4824.

Table 1. Crystal Data for $[Ir_3S_2CH_2CN_3]BPh_4 \cdot CH_3COCH_3$[a]

formula	$C_{59}H_{73}BIr_3NOS_2$	β, deg	101.15(2)
fw	1463.8	V, Å^3	5712(1)
cryst syst	monoclinic	Z	4
space group	$P2_1/c$	R, R_w	0.051, 0.041
color of crystal	reddish orange	GOF	1.29
a, Å	15.994(4)		
b, Å	12.302(2)		
c, Å	29.589(6)		

[a] $R = [\sum||F_o| - |F_c||/\sum|F_o|]$; $R = [\sum|w|F_o| - |F_c||^2/\sum w|F_o|^2)^{1/2}$, where $w = 1/\sigma^2(F_o)$; GOF $= [w(|F_o| - |F_c|)^2/(m - n)]^{1/2}$, where m denotes the number of independent observed data and n denotes the number of refined parameters.

solution of the complex. A reddish orange prismatic crystal having dimensions of 0.25 × 0.25 × 0.10 mm was mounted on glass fiber with epoxy resin. The reflections were collected by the ω scan technique ($2° < 2\theta < 55°$) on a Rigaku AFC5R diffractometer with graphite monochromated Mo Kα radiation. The 4053 independent reflections with $I > 3\sigma(I)$ were used for the structure refinements. All of the calculations were carried out on a Silicon Graphics IRIS indigo computer system using TEXSAN.[17] The structure was solved by direct methods and expanded using Fourier and difference Fourier techniques. An acetone molecule was found in the difference Fourier map as a crystal solvent. Empirical absorption corrections were performed with the program DIFABS,[18] resulting in transmission factors ranging from 0.64 to 1.25. Non-hydrogen atoms were refined anisotropically, and the hydrogen atoms were placed in idealized positions in the cation part, $[(Ir(\eta^5\text{-}C_5Me_5))_2(Ir(\eta^4\text{-}C_5Me_5)CH_2CN)(\mu_3\text{-}S)_2]^+$. The phenyl rings of tetraphenylborate were treated as rigid groups together with their hydrogen atoms. The crystal solvent, acetone, was refined isotropically, and their hydrogen atoms were not included in the calculation. Refinements were carried out using full-matrix least-squares procedures. The data for crystal structure analysis are shown in Table 1.

Reduction of Carbon Dioxide. The electrochemical reduction of CO_2 was carried out under controlled potential electrolysis conditions in a CO_2-saturated CH_3CN solution containing $[(Ir(\eta^5\text{-}C_5Me_5))_3(\mu_3\text{-}S)_2](BPh_4)_2$ or $[(Ir(\eta^5\text{-}C_5Me_5))_2(Ir(\eta^4\text{-}C_5Me_5)CH_2CN)(\mu_3\text{-}S)_2](BPh_4)$ in the presence of Me_4NBF_4 as a supporting electrolyte. The electrolysis cell was composed of three compartments: a glassy carbon working electrode (2.0 cm^2), a Pt- or an Mg-wire auxiliary electrode, and an Ag|AgCl reference electrode.[19] The working electrode compartment was connected to a volumetric flask filled with Nujol through a stainless steel tube. The solutions were saturated with CO_2 by bubbling for 30 min. The electrolysis was performed with a Hokuto Denko HA-501 potentiostat, and the electricity consumed was measured with a Hokuto Denko HF-201 Coulomb meter.

Product Analysis. Gaseous products were sampled from the gaseous phase with a pressure-locked syringe at a fixed interval of electricity consumed in the electrolysis and analyzed on a Shimadzu GC-8A gas chromatograph equipped with a 2 m column filled with Molecular Sieve 13X using He as a carrier gas at 40 °C. After the electrolysis, the amount of $HCOO^-$ in solutions and $C_2O_4^{2-}$ deposited on the working electrode cell were determined with a Shimadzu IP-3A isotachophoretic analyzer. The ^{13}C NMR spectrum of the white solid deposited in the electrolysis showed a signal at δ 160 ppm of $C_2O_4^{2-}$ in D_2O. The formation of $C_2O_4^{2-}$ was also confirmed as follows; an aqueous HCl solution (0.1 N, 10 cm^3) was added to crude orange mixtures obtained by evaporation of the solvent in vacuo. Protonated products were extracted with diethyl ether (5 cm^3) and then converted into the corresponding methyl esters by treatment with CH_2N_2 at 0 °C. The ether solution was analyzed by a Shimadzu GCMS-QP1000EX equipped with a 20 m capillary column at 40−200 °C using He as a carrier gas by comparing the retention time and the parent peak (m/z: 119 (M + H)) of the authentic sample.

(17) *TEXSAN: Single Crystal Structure Analysis Software*, Version 1.6; Molecular Structure Corp.: The Woodlands, TX,1993.
(18) DIFABS: Walker, N.; Stuart, D. *Acta Crystallogr.* **1983**, *A39*, 158.
(19) A difference in counter electrodes between Pt and Mg did not give a serious effect on the electrochemical reduction of CO_2.

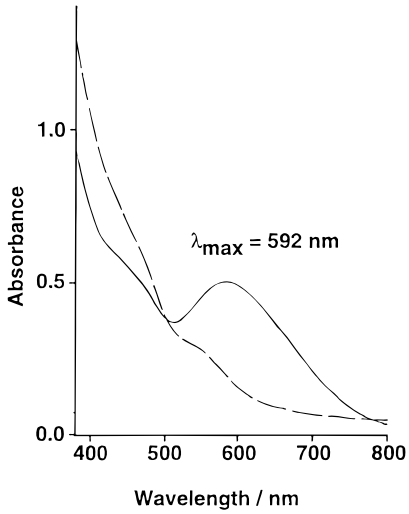

Figure 1. Electronic absorption spectra of $[Ir_3S_2]^0$ before (—) and after the reaction with CO_2 (- -) in CH_3CN.

IR Spectra under Electrolysis Conditions. Solution IR spectra under electrolysis conditions were obtained by using a KBr cell equipped with a spacer made of Novix films (purchased from Iwaki Co., Ltd.), an Au mesh for a working electrode, a Pt wire for an auxiliary electrode, and a luggin capillary to separate a reference electrode from the working electrode.[10] The thickness of the cell was 0.3 mm, and the total cell volume was 0.1 cm^3. A CD_3CN solution containing a metal complex (1×10^{-2} M) and $LiBF_4$ (5×10^{-2} M) in the IR cell was continuously cooled by refrigerants and exposed to an IR ray only on measuring to prevent the evaporation of CO_2 from the solution.

Results and Discussion

Electrochemical Reduction of CO_2 in the Presence of $[(Ir(\eta^5\text{-}C_5Me_5))_3(\mu_3\text{-}S)_2]^{2+}$. The cyclic voltammogram (CV) of $[(Ir(\eta^5\text{-}C_5Me_5))_3(\mu_3\text{-}S)_2](BPh_4)_2$ ($[Ir_3S_2]^{2+}$) in CH_3CN displayed two reversible $[Ir_3S_2]^{2+/+}$ and $[Ir_3S_2]^{+/0}$ redox couples at $E_{1/2} = -0.83$ V, ($E_{cp} = -0.86$ V, $E_{ap} = -0.80$ V) and −0.98 V ($E_{cp} = -1.01$ V, $E_{ap} = -0.95$ V) under N_2.[16] These redox waves were hardly influenced by an introduction of CO_2. Cathodic polarization of $[Ir_3S_2]^{2+}$ at −1.30 V for 3 min under N_2 and CO_2 also gave the similar $[Ir_3S_2]^{2+/+}$ and $[Ir_3S_2]^{+/0}$ anodic peaks in the reverse potential sweep. On the other hand, an introduction of CO_2 into the CH_3CN solution of $[Ir_3S_2]^0$, which was prepared by two-electron reduction of $[Ir_3S_2](BPh_4)_2$ at −1.30 V, resulted in a rapid color change from blue to orange (Figure 1). Both $(Me_4N)_2C_2O_4$ and $[(Ir(\eta^5\text{-}C_5Me_5))_2(Ir(\eta^4\text{-}C_5Me_5)\text{-}CH_2CN)((\mu_3\text{-}S)_2](BPh_4)$ ($[Ir_3S_2CH_2CN](BPh_4)$) (*vide infra*) were obtained from the yellow solution in 40 and 44% yields, respectively, based on $[Ir_3S_2]^0$. The spectrum of a dashed line of Figure 1 was consistent with that of $[Ir_3S_2CH_2CN](BPh_4)$. The controlled potential electrolysis of $[Ir_3S_2](BPh_4)_2$ (0.50 mmol/dm^3) with Me_4NBF_4 (50 mmol/dm^3) in CO_2-saturated CH_3CN at −1.30 V almost stopped after the complex underwent two-electron reduction, while the same electrolysis conducted at −1.60 V catalytically produced $(Me_4N)_2C_2O_4$ as a white precipitate. Although the rate of the reduction of CO_2 gradually slowed due to the deposition of $(Me_4N)_2C_2O_4$ on a glassy carbon electrode, replacement of the electrode by a new one reproduced the initial reaction rate of the CO_2 reduction. On the basis of the amount of $(Me_4N)_2C_2O_4$ deposited in the electrolysis cell, the current efficiency for the $C_2O_4^{2-}$ generation was 60% after 60 C passed (eq 4). Neither CO nor CO_3^{2-} was produced in

$$2CO_2 + 2e^- \rightarrow C_2O_4^{2-} \quad (4)$$

Table 2. Selected Interatomic Distances (Å) and Angles (deg) for $[Ir_3S_2CH_2CN]BPh_4 \cdot CH_3COCH_3$

Ir1−Ir2	2.912(2)	Ir1−Ir3	2.879(1)
Ir2−Ir3	2.822(1)	Ir1−S1	2.289(5)
Ir1−S2	2.287(5)	Ir2−S1	2.291(5)
Ir2−S2	2.300(5)	Ir3−S1	2.297(5)
Ir3−S2	2.299(4)	Ir1−C1	2.65(2)
Ir1−C2	2.18(2)	Ir1−C3	2.12(2)
Ir1−C4	2.09(2)	Ir1−C5	2.19(2)
Ir2−C13	2.14(2)	Ir2−C14	2.18(2)
Ir2−C15	2.21(2)	Ir2−C16	2.16(2)
Ir2−C17	2.15(2)	Ir3−C23	2.24(2)
Ir3−C24	2.21(2)	Ir3−C25	2.18(2)
Ir3−C26	2.20(2)	Ir3−C27	2.18(2)
C1−C2	1.54(3)	C2−C3	1.49(3)
C3−C4	1.37(3)	C4−C5	1.43(3)
C1−C5	1.50(3)	C1−C6	1.54(3)
C1−C7	1.61(3)	C7−C8	1.49(3)
C8−N1	1.16(3)	C13−C14	1.39(3)
C14−C15	1.39(3)	C15−C16	1.41(3)
C16−C17	1.43(3)	C17−C13	1.39(3)
C23−C24	1.44(3)	C24−C25	1.45(3)
C25−C26	1.46(3)	C26−C27	1.41(3)
C27−C23	1.43(4)		
Ir2−Ir1−Ir3	58.32(3)	Ir1−Ir2−Ir3	60.26(3)
Ir1−Ir3−Ir2	61.42(3)	S1−Ir1−S2	87.7(2)
S1−Ir2−S2	87.3(2)	S1−Ir3−S2	87.2(2)
Ir1−S1−Ir2	79.0(2)	Ir1−S1−Ir3	77.8(2)
Ir2−S1−Ir3	75.9(2)	Ir1−S2−Ir2	78.8(2)
Ir1−S2−Ir3	77.8(2)	Ir2−S2−Ir3	75.7(2)
C2−C1−C5	100(1)	C1−C2−C3	101(1)
C2−C3−C4	110(1)	C3−C4−C5	107(1)
C1−C5−C4	107(1)	C2−C1−C6	113(1)
C2−C1−C7	115(1)	C5−C1−C6	112(1)
C5−C1−C7	111(1)	C6−C1−C7	103(1)
C1−C7−C8	111(1)	N1−C8−C7	176(2)
C14−C13−C17	110(1)	C13−C14−C15	106(1)
C14−C15−C16	109(1)	C15−C16−C17	106(1)
C13−C17−C16	106(1)	C24−C23−C27	105(1)
C23−C24−C25	106(1)	C24−C25−C26	111(1)
C25−C26−C27	102(2)	C23−C27−C26	114(2)

the electrolysis (GC and IR analysis), but small amounts of $HCOO^-$ (less than 60% based on $[Ir_3S_2]^{2+}$) was detected in the solution after the electrolysis. Exposure of the electrolyte solution to air after the electrolysis gave the electronic absorption spectrum of $[Ir_3S_2CH_2CN](BPh_4)$ (a dashed line in Figure 1). In accord with this, the similar electrochemical reduction of CO_2 in the presence of $[Ir_3S_2CH_2CN](BPh_4)$ (0.50 mmol/dm^3) at −1.60 V in CH_3CN also generated oxalate with a current efficiency of 64% and a turnover number was 5.4/h in the electrolysis for 10 h. The electronic absorption spectrum of $[Ir_3S_2CH_2CN]^+$ was also regenerated by exposure of the final electrolyte solution to air. These results clearly indicate that $[Ir_3S_2]^{2+}$ is converted to $[Ir_3S_2CH_2CN]^+$ with generation of $C_2O_4^{2-}$ in CO_2-saturated CH_3CN under the electrolysis at −1.30 V, and the resultant $[Ir_3S_2CH_2CN]^+$ works as an active species for the catalytic formation of $C_2O_4^{2-}$ in the electrochemical reduction of CO_2 at −1.60 V.

Structure of $[(Ir(\eta^5\text{-}C_5Me_5))_2(Ir(\eta^4\text{-}C_5Me_5)CH_2CN)(\mu_3\text{-}S)_2]^+$. Figure 2 shows the ORTEP drawing of the cation part of $[Ir_3S_2CH_2CN](BPh_4)$. The selected bond distances and angles in $[Ir_3S_2CH_2CN]^+$ are listed in Table 2. Similar to the molecular structure of $[Ir_3S_2]^{2+}$,[16] the Ir_3 triangle core capped by two μ_3-S is maintained also in $[Ir_3S_2CH_2CN]^+$. Two iridium atoms, Ir2 and Ir3, are ligated by η^5-C_5Me_5 ligands, while Ir1 is ligated by an $(\eta^4\text{-}C_5Me_5)CH_2CN$ ligand. Thus, one of the three η^5-C_5Me_5 ligands in $[Ir_3S_2]^0$ was attacked by a CH_2CN group and became a tetradentate ligand, $(\eta^4\text{-}C_5Me_5)CH_2CN$. The atomic distance from C1 to Ir1 is 2.65 (2) Å, while the remaining planar C2, C3, C4, and C5 atoms of $(\eta^4\text{-}C_5Me_5)CH_2CN$ exist in the range of 2.09−2.18 Å from Ir1 (Figure 2). The bond distances

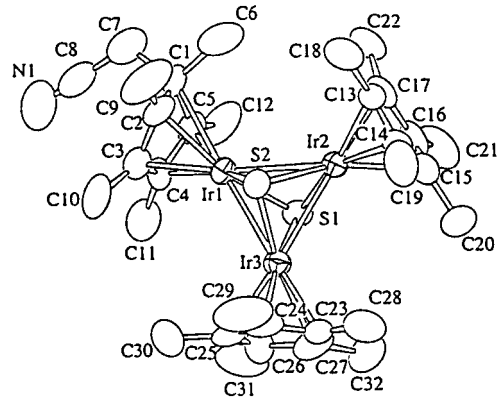

Figure 2. Molecular structure of $[(Ir(\eta^5\text{-}C_5Me_5))_2(Ir(\eta^5\text{-}C_5Me_5)CH_2CN)(\mu_3\text{-}S)_2]^+$.

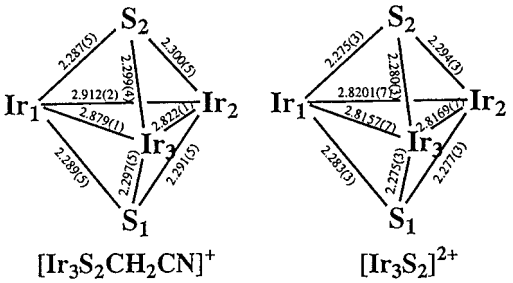

Figure 3. Ir_3S_2 cores of $[Ir_3S_2]_2^+$ and $[Ir_3S_2CH_2CN]^+$.

of Ir1−Ir2 and Ir1−Ir3 are 2.912(2) and 2.879(1) Å, respectively, and are longer than that of Ir2−Ir3 (2.822(1) Å). Since the Ir−Ir bond distances of $[Ir_3S_2]^{2+}$ are 2.816−2.820 Å (Figure 3), the oxidation states of Ir2 and Ir3 are similar to those of iridium atoms in $[Ir_3S_2]^{2+}$, while the oxidation state of Ir1 is slightly reduced.

Both Ir−Ir bond distances and the structure of the $(\eta^4\text{-}C_5Me_5)CH_2CN$ ligand indicate an increase in the electron density of Ir1 compared with those of Ir2 and Ir3 in $[Ir_3S_2CH_2CN]^+$. It is well-known that η^6-arene and η^5-C_5H_5 ligands of low-valent metal complexes are likely to undergo a ring slippage motion, which lowers the ligand hapticity to avoid accumulation of too much electrons in metal centers.[20] The present study is the first example of the change of the coordination mode from η^5- to η^4-C_5Me_5 by an attack of solvent CH_3CN. Fujita and Creutz proposed an oxidative addition of CD_3CN to tetraazamacrocyclic Co(I) complexes affording $[Co^{III}(D)(CD_2CN)]$ as an active species for an H/D exchange reaction between NH protons of the ligands and solvent CD_3CN.[21] An oxidative addition of CH_3CN to an Ir atom of $[Ir_3S_2]^0$ followed by an intramolecular rearrangement of CH_2CN bonded to Ir to a η^5-C_5Me_5 ligand in the $(Ir(\eta^5\text{-}C_5Me_5))_3(\mu_3\text{-}S)_2$ framework is supposed to produce an *endo*-$(\eta^4\text{-}C_5Me_5)CH_2CN$ isomer. However, only the *exo*-$(\eta^4\text{-}C_5Me_5)CH_2CN$ form was isolated. The ^{1}H NMR spectra of $[Ir_3S_2CH_2CN](BPh_4)$ also showed a singlet signal of *exo*-CH_2CN at δ 0.08, and an endo isomer was not detected up to −90 °C in CD_2Cl_2. Moreover, CO_2 is the essential component for the formation of $[(Ir(\eta^5\text{-}C_5Me_5))_2(Ir(\eta^4\text{-}C_5Me_5)CH_2CN)(\mu_3\text{-}S)_2]^+$ (eq 5), since blue $[Ir_3S_2]^0$ was stable in CH_3CN under

$$[(Ir(\eta^5\text{-}C_5Me_5)CH_2CN)_3(\mu_3\text{-}S)_2]^0 + CO_2 \xrightarrow{CH_3CN} [(Ir(\eta^5\text{-}C_5Me_5))_2(Ir(\eta^4\text{-}C_5Me_5)CH_2CN)(\mu_3\text{-}S)_2]^+ + C_2O_4^{2-} \quad (5)$$

(20) Geiger, W. E. *Acc. Chem. Res.* **1995**, *28*, 351.
(21) Fujita, E.; Creutz, C. *Inorg. Chem.* **1994**, *33*, 1729.

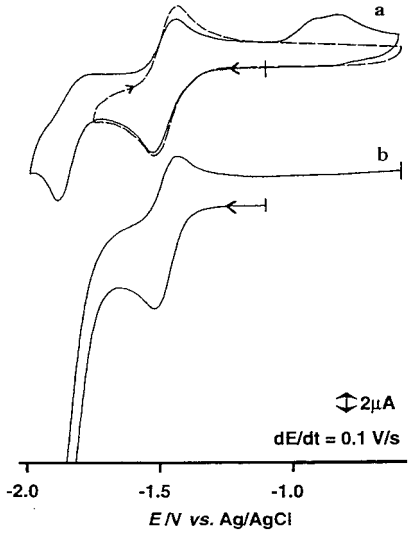

Figure 4. Cyclic voltammograms of $[Ir_3S_2CH_2CN](BPh_4)$ in CH_3CN under N_2 (a) and CO_2 (b). $dE/dt = 100$ mV/s.

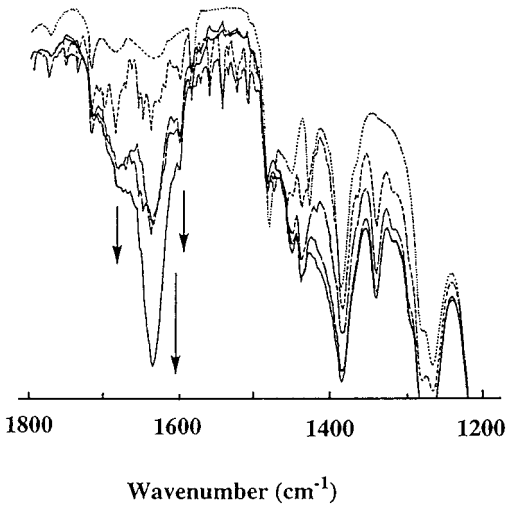

Figure 5. Time course of the IR spectra of $[Ir_3S_2](BPh_4)_2$ in CO_2-saturated CD_3CN under the electrolysis at -1.55 V (from top to bottom lines).

N_2. The elucidation of the mechanism for the reaction of eq 5 including the role of CO_2 is currently under way.

Redox Behavior of $[Ir_3S_2CH_2CN]^+$ as Active Species for Oxalate Formation. The CV of $[Ir_3S_2CH_2CN](BPh_4)$ in CH_3CN shows a pseudoreversible $[Ir_3S_2CH_2CN]^{+/0}$ couple at $E_{1/2} = -1.45$ V ($E_{cp} = -1.49$ V, $E_{ap} = -1.40$ V) under N_2 (a broken line in Figure 4a). When the potential range is spread to -2.0 V, an irreversible anodic wave appears at $E_{cp} = -1.83$ V and two anodic waves emerge at -0.78 and -0.93 V at the expense of the anodic peak current at -1.45 V in the reverse potential scanning (Figure 4b). The peak potentials and the patterns of the -0.78 and -0.93 V anodic waves are consistent with those of the anodic ones of the $[Ir_3S_2]^{0/+/2+}$ redox couples. Thus, $[Ir_3S_2]^0$ is obviously regenerated by dissociation of the CH_2CN^- group upon two-electron reduction of $[Ir_3S_2CH_2CN]^+$ (eqs 6, 7). On the other hand, the CV of $[Ir_3S_2CH_2CN]^+$ under CO_2

$$[Ir_3S_2CH_2CN]^+ + e^- \rightleftharpoons [Ir_3S_2CH_2CN]^0 \quad (6)$$

$$[Ir_3S_2CH_2CN]^0 + e^- \rightarrow [Ir_3S_2]^0 + [CH_2CN]^- \quad (7)$$

showed a strong catalytic current due to the reduction of CO_2 at potentials more negative than the cathodic wave of the $[Ir_3S_2CH_2CN]^{0/-}$ couple (Figure 4b). Moreover, the -0.78 and -0.93 V anodic waves of the $[Ir_3S_2]^{2+/+/0}$ redox couples do not emerge in the reverse potential scanning under CO_2, suggesting that electrons transferred to $[Ir_3S_2CH_2CN]^0$ were effectively consumed in the reduction of CO_2, affording $C_2O_4^{2-}$ without dissociating the CH_2CN group. Indeed, the electronic absorption spectrum of $[Ir_3S_2CH_2CN]^+$ was maintained after the electrochemical reduction of CO_2 catalyzed by $[Ir_3S_2CH_2CN]^+$ in CH_3CN, and $NCCH_2COO^-$ was not detected in the final electrolyte solution. Thus, $[Ir_3S_2CH_2CN]^+$ stably works as an active species for the generation of $C_2O_4^{2-}$ in the CO_2 reduction. On the other hand, treatments of $[Ir_3S_2CH_2CN]^+$ with aqueous HCl in CH_3CN and dimethyl sulfoxide (DMSO) quantitatively produced $[Ir_3S_2]^{2+}$ and CH_3CN (eq 8).

$$[Ir_3S_2CH_2CN]^+ + H^+ \rightarrow [Ir_3S_2]^{2+} + CH_3CN \quad (8)$$

IR Spectra of CO_2 Adducts. The electrochemical reduction of $[Ir_3S_2]^{2+}$ and $[Ir_3S_2CH_2CN]^+$ in CO_2-saturated CD_3CN was monitored by IR spectra. Blank electrolysis of CO_2-saturated CD_3CN in the presence of Me_4NBF_4 at -1.50 V in a thin layer IR cell (see Experimental Section) did not cause any changes in the IR spectra. On the other hand, when the given potential became -2.0 V,[22] $(Me_4N)_2C_2O_4$ deposited on an IR window and two bands gradually appeared at 1633 (s) and 1397 (m) cm^{-1}. The IR spectra of $[Ir_3S_2](BPh_4)_2$ in CD_3CN did not show any interaction with CO_2. The controlled potential electrolysis of the solution at -1.50 V in CO_2-saturated CD_3CN brings about an appearance of the 1633 cm^{-1} band of $(Me_4N)_2C_2O_4$ with two other bands around 1680 and 1600 cm^{-1} in the initial stage of the reduction (Figure 5). The growth of the 1680 and 1600 cm^{-1} bands became gradually slow, and the 1633 cm^{-1} band of $(Me_4N)_2C_2O_4$ kept on growing during the electrolysis (Figure 5). The appearance of three bands at 1680, 1633, and 1600 cm^{-1} was more clearly observed in the reduction of CO_2 by $[Ir_3S_2CH_2CN](BPh_4)$ under similar electrolysis conditions. A CD_3CN solution containing $[Ir_3S_2CH_2CN](BPh_4)$ and $LiBF_4$ did not show any bands around 1700 cm^{-1} under N_2. An introduction of CO_2 to the solution brought about an appearance of the 1682 cm^{-1} band with a weak band at 1337 cm^{-1} (Figure 6). Recovery of $[Ir_3S_2CH_2CN]^+$ by evaporation of the solvent is indication of a reversible CO_2 adduct formation with the $\nu(CO_2)$ band at 1682 cm^{-1} (eq 9). Moreover, when $[Ir_3S_2CH_2CN]^+$ was reduced electrochemically at -1.50 V in CO_2-saturated CD_3CN, a band at 1603 cm^{-1} gradually emerged in addition to the strong band centered at 1680 cm^{-1} (Figure 6). After the 1603 cm^{-1} band reached to a certain intensity in the electrolysis, the 1633 cm^{-1} band of $C_2O_4^{2-}$ emerged and increased continuously. Prolonged electrolysis of $[Ir_3S_2CH_2CN](BPh_4)$ in CO_2-saturated CD_3CN gave the almost same IR spectra as those in Figure 5 (IR spectra of the final stage of the electrolysis were omitted in Figure 6 in order to clarify the spectral changes in the initial stage of the electrolysis). Reoxidation of the solution at 0 V resulted in disappearance of only the 1603 cm^{-1} band, and the IR bands resulting from the

$$[Ir_3S_2CH_2CN]^+ + CO_2 \rightleftharpoons \{[Ir_3S_2CH_2CN](CO_2)\}^+ \quad (9)$$

(22) (a) Bard, A. J., Parsons, R., Jordan, J., Eds. *Standard Potentials in Aqueous Solution*; IUPAC, Physical and Analytical Chemistry Divisions, Marcel Dekker: New York, 1985. (b) Latimer, W. L. *The Oxidation States of the Elements and Their Potentials in Aqueous Solutions*, 2nd ed.; Prentice Hall: Englewood Cliffs, NJ, 1952.

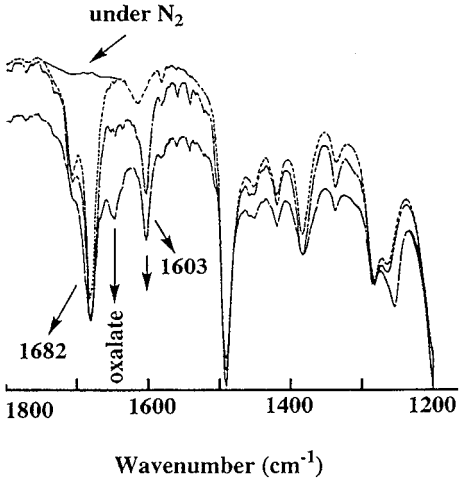

Figure 6. IR spectra of $[Ir_3S_2CH_2CN](BPh_4)$ in CD_3CN (the top line) and time course of the spectra in CO_2-saturated CD_3CN under the electrolysis at −1.55 V (from the second to bottom lines).

CO_2 adduct (a strong band centered at 1680 cm^{-1}) and $C_2O_4^{2-}$ (1633 cm^{-1}) remained. The peak intensity of the 1603 cm^{-1} band grows until the 1633 cm^{-1} band ($C_2O_4^{2-}$) emerged in the electrolysis of $[Ir_3S_2CH_2CN]^+$ in CO_2-saturated CD_3CN, and the peak intensity of the band centered at 1680 cm^{-1} is almost unchanged (Figure 6). The small shift of the $\nu(CO_2)$ band from 1682 to 1680 cm^{-1} in the reduction of $[Ir_3S_2CH_2CN]^+$ under CO_2 is neglected by considering the resolution of the spectrophotometer. The 1603 cm^{-1} band, therefore, is associated with either the bathochromic shift of the 1682 cm^{-1} band upon one-electron reduction of the cationic $\{[Ir_3S_2CH_2CN](CO_2)\}^+$ (eq 10) or a 1:2 adduct formed by an attack of a second CO_2

$$\underset{1682\ cm^{-1}}{\{[Ir_3S_2CH_2CN](CO_2)\}^+} + e^- \rightleftharpoons \underset{1603\ cm^{-1}}{\{[Ir_3S_2CH_2CN](CO_2)\}^0} \quad (10)$$

$$\underset{1682\ cm^{-1}}{\{[Ir_3S_2CH_2CN](CO_2)\}^+} + CO_2 + e^- \rightleftharpoons \underset{1680\ \text{and}\ 1603\ cm^{-1}}{\{[Ir_3S_2CH_2CN](CO_2)_2\}^0} \quad (11)$$

molecule to the one-electron reduced form of $\{[Ir_3S_2CH_2CN](CO_2)\}^+$ under CO_2 (eq 11). There is no doubt that a second CO_2 must be activated prior to the formation of $C_2O_4^{2-}$ by considering the difficulty of the oxalate formation by the direct reaction of $\{[Ir_3S_2CH_2CN](CO_2)\}^-$ with free CO_2. It is, however, not necessarily the involvement of a stable 1:2 adduct of neutral $\{[Ir_3S_2CH_2CN](CO_2)_2\}^0$ (eq 11). If regeneration of $[Ir_3S_2CH_2CN]^+$ in the catalytic cycle of the $C_2O_4^{2-}$ production is fast enough compared with the reactions of eqs 9 and 10, the 1682 cm^{-1} band of $\{[Ir_3S_2CH_2CN](CO_2)\}^+$ (eq 9) must remain in the IR spectra during the electrolysis at −1.55 V under CO_2. On the other hand, even if both the cationic 1:1 adduct of $\{[Ir_3S_2CH_2CN](CO_2)\}^+$ and the neutral 1:1 one of $\{[Ir_3S_2CH_2CN](CO_2)\}^0$ show the $\nu(CO_2)$ band at 1682 cm^{-1}, possibly due to ligation of CO_2 to a site remote from the redox center, the peak intensity and/or the wavenumber of the band must be influenced by an attack of the second CO_2 to the neutral $\{[Ir_3S_2CH_2CN](CO_2)\}^0$ (eq 11). The change in the IR spectra of the electrolysis of $[Ir_3S_2CH_2CN]^+$ under CO_2 at −1.55 V (Figure 6), therefore, is explained by the formation of $\{[Ir_3S_2CH_2CN](CO_2)\}^0$ (eq 10) rather than $\{[Ir_3S_2CH_2CN](CO_2)_2\}^0$ (eq 11).

The IR spectra of $[Ir_3S_2CH_2CN](BPh_4)$ in $^{13}CO_2$-saturated CD_3CN also exhibited two $\nu(^{13}CO_2)$ bands at 1632 and 1317 cm^{-1}. Besides these bands, electrolysis of the solution at −1.50 V gave rise to the appearance of a new $\nu(^{13}CO_2)$ band at 1561 cm^{-1},[23] and then the strong $\nu(^{13}CO_2)$ bands of $C_2O_4^{2-}$ appeared at 1601 and 1366 cm^{-1}. On the basis of these spectral changes, the $\nu(^{13}CO_2)$ modes of a 1:1 adduct between $[Ir_3S_2CH_2CN]^+$ and CO_2 (eq 9) is assigned to the band at 1632 cm^{-1}. One-electron reduction of $[Ir_3S_2CH_2CN]^+$ under $^{13}CO_2$ caused an appearance of a $\nu(^{13}CO_2)$ band at 1561 cm^{-1}, which is assigned to the adduct between $[Ir_3S_2CH_2CN]^0$ and $^{13}CO_2$ (eq 10).

The possible binding modes for the reversible addition of CO_2 to $[Ir_3S_2CH_2CN]^+$ is either an η^1- or η^2-CO_2 bond. Metal complexes with an η^1- and η^2-CO_2 group usually display two characteristic stretching bands in the IR spectra; $\nu_{asym}(CO_2)$ and $\nu_{sym}(CO_2)$ bands of η^1-CO_2 complexes are observed at 1428−1650 and 1210−1280 cm^{-1}, respectively.[24] On the other hand, $\nu(C{=}O)$ and $\nu(C{-}O)$ bands of η^2-CO_2 complexes emerge at 1630−1745 and 1100−1155 cm^{-1}, respectively.[25] The IR spectrum of $[Ir_3S_2CH_2CN]^+$ in CO_2-saturated CD_3CN (eq 9) showed the $\nu(^{12}CO_2)$ bands at 1682 (s) and 1337 cm^{-1}. One-electron reduction of the cationic CO_2 adduct exhibited $\nu(^{12}CO_2)$ band at 1603 cm^{-1} (eq 10). Thus, CO_2 molecules are concluded to be linked to $[Ir_3S_2CH_2CN]^{n+}$ ($n = 0$ and 1) with an η^1-CO_2 mode. The catalytic currents detected in the CV of $[Ir_3S_2CH_2CN]^+$ under CO_2 (Figure 4b), therefore, are caused by irreversible reduction of $\{[Ir_3S_2CH_2CN](\eta^1\text{-}CO_2)\}^0$, affording oxalate (eq 12). Although oxalate generation has been reported in the

$$\{[Ir_3S_2CH_2CN](CO_2)\}^0 + CO_2 + e^- \rightarrow [Ir_3S_2CH_2CN]^+ + C_2O_4^{2-} \quad (12)$$

controlled potential electrolysis of octaethylporphyrin Pd and Ag complexes in CH_2Cl_2 at −1.50 V under CO_2 atmosphere,[26] activation of one CO_2 molecule on electrochemically reduced metal centers usually produces CO and CO_3^{2-} under aprotic conditions (eq 2). Indeed, a smooth C−O bond cleavage is shown in the electrochemical reduction of CO_2 by Fe(0) porphirins.[8,27]

Activation of CO_2 on $[Ir_3S_2CH_2CN]^{n+}$. The complete depression of the reductive disproportionation reaction of CO_2 affording CO and CO_3^{2-} (eq 2) in the electrochemical reduction of CO_2 by $[Ir_3S_2CH_2CN]^+$ would be ascribed to both the weak basicity of the CO_2 molecules and the binding site of $[Ir_3S_2CH_2CN]^+$. An oxide transfer reaction from metal−η^1-CO_2 to

(23) One of the $\nu_{sym}(CO_2)$ bands of $[Ir_3S_2CH_2CN](CO_2)_2$ was not detected, probably due to overlap of other vibrational bands.

(24) (a) Gambarotta, S.; Arena, F.; Floriani, C.; Zanazzi, P. F. *J. Am. Chem. Soc.* **1982**, *104*, 5914. (b) Calabrese, J. C.; Herskovitz, T.; Kinney, J. B. *J. Am. Chem. Soc*. **1983**, *105*, 5914.

(25) (a) Aresta, M.; Nobile, C. F. *J. Chem. Soc., Dalton Trans*. **1977**, 708. (b) Aresta, M.; Nobile, C. F.; Albano, F. G.; Forni, E.; Manassero, M. *J. Chem. Soc., Chem. Commun*. **1975**, 636. (c) Komiya, S.; Akita, M.; Kasuga, N.; Hirano, M.; Fukuoka, A. *J. Chem. Soc., Chem. Commun*. **1994**, 1115. (d) Gambarotta, B.; Floriani, C.; Chiesi-Villa, A.; Guastini, C. *J. Am. Chem. Soc*. **1985**, *107*, 2985. (e) Brisrow, G. S.; Hitchcock, P. B.; Lappert, M. F. *J. Chem. Soc., Chem. Commun*. **1981**, 1145. (f) Alvarez, R.; Carmona, E.; Marin, J. M.; Poveda, M. L.; Gutierrez-Puebla, E.; Monge, A. *J. Am. Chem. Soc*. **1986**, *108*, 2286. (g) Alvarez, R.; Atwood, J. L.; Carmona, E.; Perez, P. J.; Poveda, M. L.; Rogers, R. D. *Inorg. Chem*. **1991**, *30*, 1493.

(26) Becker, J. Y.; Vainas, B.; Eger, R.; Kaufman, L. *J. Chem. Soc., Chem. Commun*. **1985**, 1471.

(27) Grodkowski, J.; Behar, D.; Nata, P.; Hambright, P. *J. Phys. Chem. A* **1997**, *101*, 248.

Scheme 1

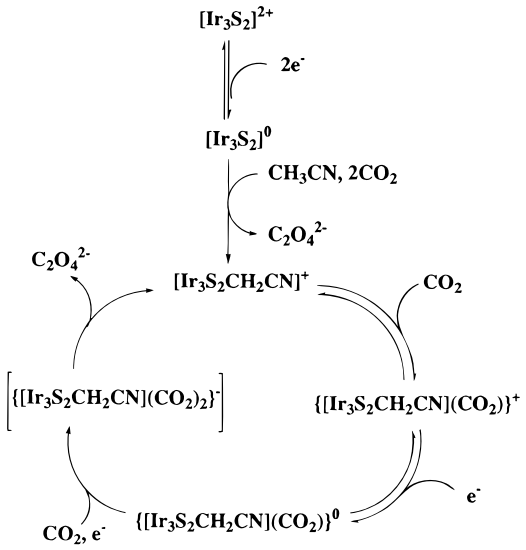

CO_2 is effectively accelerated with an increase of the basicity of the η^1-CO_2 group,[10] which is primarily dependent on the electron donating ability of central metals. An OCO angle of η^1-CO_2 adducts is reasonably correlated with the electron density of the group. For example, ammonia and anionic imidazolidone as weak and strong bases, respectively, form the 1:1 adduct with CO_2, and the OCO angles of H_3NCO_2[28] and [OOCNC(O)-$NHCH_2CH_2]^-$ [29] are almost linear and 132°, respectively. The close similarity of the latter with those of [Co(Pr(salen))(η^1-CO_2Na)]$^+$ (135°),[24a] and [RhCl(diars)(η^1-CO_2)] (126°)[24b] indicates that CO_2 bonded to strong organic bases also can reductively activate CO_2 similar to metal−η^1-CO_2 complexes. It is possible to assay the OCO angle of an η^1-CO_2 adduct under the assumption that $\nu(CO_2)$ bands are not seriously coupled with other vibrational modes. An OCO angle (2α) of an η^1-CO_2 moiety is expressed by using eq 13,[30] in which ν^i and ν represent

$$\left(\frac{\nu^i}{\nu}\right)^2 = \left(\frac{M_c}{M_c^i}\right)\left(\frac{M_c^i + 2M_o \sin^2 \alpha}{M_c + 2M_o \sin^2 \alpha}\right) \qquad (13)$$

the $\nu_{asym}(^{13}CO_2)$ and $\nu_{asym}(^{12}CO_2)$ bands (cm^{-1}), and M_c^i, M_c, and M_o are the mass number of ^{13}C, ^{12}C, and ^{16}O, respectively. The IR spectra of $[Ir_3S_2CH_2CN]^+$ in $^{12}CO_2$-saturated CD_3CN displayed a $\nu_{asym}(^{12}CO_2)$ band at 1682 cm^{-1} (eq 9), and electrochemical reduction of $[Ir_3S_2CH_2CN]^+$ showed the $\nu_{asym}(^{12}$-$CO_2)$ band at 1603 cm^{-1} (eq 10). These $\nu_{asym}(^{12}CO_2)$ bands at 1682 and 1603 cm^{-1} shifted to 1632 and 1561 cm^{-1}, respectively, in $^{13}CO_2$-saturated CD_3CN. On the basis of these ν_{asym}-(CO_2) bands, the OCO angles of the CO_2 molecules bonded to $[Ir_3S_2CH_2CN]^+$ and $[Ir_3S_2CH_2CN]^0$ are calculated as 157 and 132°, respectively. Thus, CO_2 ligated on $[Ir_3S_2CH_2CN]^0$ accepts more electrons than that on $[Ir_3S_2CH_2CN]^+$.

Scheme 1 represents the most possible reaction path for the generation of $C_2O_4^{2-}$ in the electrochemical reduction of CO_2 in the presence of $[Ir_3S_2]^{2+}$. Two-electron reduction of $[Ir_3S_2]^{2+}$ at −1.30 V in CH_3CN under CO_2 atmosphere results in the formation of $C_2O_4^{2-}$ and $[Ir_3S_2CH_2CN]^+$, the latter of which, however, is hardly reduced at the potential. Thus, irrespective of the catalytic ability of $[Ir_3S_2]^0$ for the reduction of CO_2, $[Ir_3S_2]^{2+}$ is completely converted to $[Ir_3S_2CH_2CN]^+$ under the electrolysis at −1.30 V in CO_2-saturated CH_3CN. The rate of the reduction of CO_2 by $[Ir_3S_2CH_2CN]^+$ greatly increases when the electrolysis is conducted at potentials more negative than −1.8 V (Figure 5b). However, the IR spectra showed the formation of $C_2O_4^{2-}$ under the electrolysis at −2.0 V even in the absence of $[Ir_3S_2CH_2CN]^+$ in CH_3CN under CO_2. Moreover, aromatic anion radicals with the redox potentials more negative than −1.93 V (*vs* SCE) assists the formation of CO_2^- as a precursor to $C_2O_4^{2-}$ in electrochemical CO_2 reduction. The electrochemical reduction of CO_2 catalyzed by $[Ir_3S_2CH_2CN]^+$, therefore, was conducted at −1.60 V to exclude the possibility of the formation of free CO_2^- either by direct reduction of CO_2 on an electrode or by a trace amount of impurity involved in the electrolyte. Air oxidation of the CH_3CN solution after the electrochemical reduction of CO_2 catalyzed by $[Ir_3S_2CH_2CN]^+$ at −1.60 V regenerated the electronic absorption spectrum of $[Ir_3S_2CH_2CN]^+$. Thus, the Ir cluster stably works as an active species for the generation of $C_2O_4^{2-}$.

A direct attack of CO_2 to Ir of $[Ir_3S_2CH_2CN]^+$ would be blocked by η^5-C_5Me_5, (η^4-C_5Me_5)CH_2CN, and μ_3-S ligands, while there seems to be no serious steric hindrance for an electrophilic attack of CO_2 to a μ_3-S ligand. Although a protolysis reaction of $[Ir_3S_2CH_2CN]^+$ producing $[Ir_3S_2]^{2+}$ and CH_3CN (eq 8) made it difficult to determine the basicity (pK_a) of a μ_3-S ligand of $[Ir_3S_2CH_2CN]^+$, the basicity of the μ_3-S ligand of $[Ir_3S_2CH_2CN]^+$ must be largely enhanced compared with that of $[Ir_3S_2]^{2+}$ due to an attachment of negatively charged CH_2CN^- to an η^5-C_5Me_5 ring of the latter. We, therefore, propose that the reversible CO_2 binding to $[Ir_3S_2CH_2CN]^+$ takes place on a μ_3-S ligand (eq 9). The resultant $\{[Ir_3S_2CH_2CN]$-$(CO_2)\}^+$ shows the $\nu(CO_2)$ band at 1683 cm^{-1}, which undergoes a bathocromic shift to 1603 cm^{-1} upon one-electron reduction of $\{[Ir_3S_2CH_2CN](CO_2)\}^+$ equilibrated with $[Ir_3S_2CH_2CN]^+$. As described in a previous section, the one-electron reduced form of $[Ir_3S_2CH_2CN]^0$ dissociates the CH_2CN group with generation of $[Ir_3S_2]^0$ under N_2 (eq 7), while it catalyzes the reduction of CO_2 to produce $C_2O_4^{2-}$ under CO_2 (Figure 4). Accordingly, one-electron reduction of $\{[Ir_3S_2CH_2CN](CO_2)\}^0$ under CO_2 must by followed by a configurational change of the Ir_3S_2 core. On the basis of a fission of a metal−metal bond of two-electron reduced forms of $[Ir_3S_2]^{2+}$ [14] and $[(Co(\eta^5\text{-}C_5H_4Me))_3(\mu_3\text{-}S)_2]^{2+}$,[31] an Ir−Ir bond cleavage is reasonably assumed to take place in $\{[Ir_3S_2CH_2CN](CO_2)\}^-$. Such an Ir−Ir bond fission would produce an open space for an electrophilic attack of the second CO_2 molecule on Ir atoms. We, therefore, conclude that the reaction of eq 12 is operative with regard to the formation of oxalate, where unstable $\{[Ir_3S_2CH_2CN](CO_2)_2\}^-$ is likely to work as the active species for the generation of oxalate. The successful generation of $C_2O_4^{2-}$ without accompanying CO evolution in the present electrochemical reduction of CO_2 catalyzed by $[Ir_3S_2CH_2CN]^+$, therefore, is ascribed to the smooth coupling reaction of two CO_2 molecules bonded on the adjacent μ_3-S and Ir atoms in $\{[Ir_3S_2CH_2CN](CO_2)\}^-$.

Supporting Information Available: Tables of crystallographic experimental details, atomic coordinates, anisotropic displacement coefficients, and interatomic distances and angles (14 pages). Ordering information is given on any current masthead page.

IC9702328

(28) Sakaki, S.; Aizawa, T.; Koga, N.; Morokuma, K.; Ohkubo, K. *Inorg. Chem.* **1989**, *28*, 103.
(29) Musashi, Y.; Hamada, T.; Sakaki, S. *J. Am. Chem. Soc.* **1995**, *117*, 11320.
(30) Nakamoto, K. *Infrared and Raman Spectra of Inorganic and Coordination Compounds*; Wiley-Interscience: New York, 1986.
(31) Pulliam, C. R.; Thoden, J. B.; Stacy, A. M.; Spencer, B.; Englert, M. H.; Dahl, L. F. *J. Am. Chem. Soc.* **1991**, *113*, 7398.